Polymer 50 (2009) 2411–2423

Contents lists available at ScienceDirect

Polymer

journal homepage: www.elsevier.com/locate/polymer

Ion–dipole interactions in the dispersion of organoclay nanocomposites based on polystyrene-*block*-poly(2-vinylpyridine) copolymer

Weibin Zha [a], Chang Dae Han [a,*], Sung Hyun Han [b], Dong Hyun Lee [b], Jin Kon Kim [b,**], Mingming Guo [c], Peter L. Rinaldi [d]

[a] *Department of Polymer Engineering, The University of Akron, 250 South Forge Street, Akron, OH 44325-0301, USA*
[b] *National Creative Research Initiative Center for Block Copolymer Self-Assembly and Chemical Engineering Department, Pohang University of Science and Technology, P.O. Box 125, Pohang, Kyungbuk 790-784, Republic of Korea*
[c] *Institute of Polymer Science, The University of Akron, Akron, OH 44325-0309, USA*
[d] *Department of Chemistry, The University of Akron, Akron, OH 44325-3601, USA*

ARTICLE INFO

Article history:
Received 17 December 2008
Received in revised form
25 February 2009
Accepted 1 March 2009
Available online 24 March 2009

Keywords:
Nanocomposites
Exfoliation
Block copolymer

ABSTRACT

The dispersion characteristics of organoclay nanocomposites based on polystyrene-*block*-poly(2-vinylpyridine) (S2VP diblock) copolymer were investigated using transmission electron microscopy (TEM), X-ray diffraction (XRD), and solid-state nuclear magnetic resonance (NMR) spectroscopy. For the investigation, S2VP diblock copolymers having three different compositions were synthesized via sequential anionic polymerization. Each S2VP diblock copolymer was used to prepare nanocomposites by solution blending with natural clay (montmorillonite, MMT) or commercial organoclays (Cloisite 30B, Cloisite 10A, Cloisite 15A, and Cloisite 25A from Southern Clay Products). All four organoclays employed were treated with a surfactant having quaternary ammonium salt with N^+ ion. It was found, via TEM and XRD, that the nanocomposites with MMT show very poor dispersion characteristics regardless of block copolymer composition. However, the block copolymer composition was found to have a profound influence on the dispersion characteristics of the nanocomposites with an organoclay. Specifically, the nanocomposites based on S2VP-5 having 5 wt% poly(2-vinylpyridine) (P2VP) block gave rise to a very high degree of dispersion, irrespective of the chemical structure of the surfactant residing at the surface of the organoclay employed, whereas the dispersion characteristics of the nanocomposites became progressively poorer as the amount of P2VP block in an S2VP diblock copolymer increased from 5 to 25 wt% and to 56 wt%. The observed dispersion characteristics were explained by hypothesizing the presence of ion–dipole interactions between the positively charged N^+ ions in the surfactant residing at the surface of the organoclay nanoparticles and the dipoles in the P2VP block of S2VP diblock copolymers. The validity of this hypothesis was confirmed using solid-state NMR spectroscopy, by determining the dependence of the composition of S2VP diblock copolymer on the extent of ion–dipole interactions and thus on the dispersion characteristics of the nanocomposites prepared.

1. Introduction

During the last fifteen years numerous research groups have reported on the preparation of organoclay nanocomposites based on various thermoplastic polymers. There are too many papers to cite them all here. For instance, according to SciFinder Scholar on the Internet, under the title of "Nanocomposites" there are over 35,000 articles that were either published in referred journals or documented in various conference proceedings. The interested readers are referred to a recent review article [1], which cited 460 papers. The ultimate goal for the preparation of organoclay nanocomposites is to achieve exfoliation of the aggregates of layered silicates by in situ polymerization, solution blending, or melt blending. More often than not, in situ polymerization for such purposes is not a practical option. Thus, when a thermoplastic polymer is mixed, via either solution blending or melt blending, with an organoclay, it either intercalates or exfoliates the aggregates of layered silicates. In general, intercalation is observed when there are insufficient attractive interactions between a polymer matrix and the layered silicates, while exfoliation is observed when a polymer matrix and the layered silicates have strong attractive interactions.

* Corresponding author. Tel.: +1 330 972 6468; fax: +1 330 972 5720.
** Corresponding author. Tel.: +82 54 279 2276; fax: +82 54 279 8298.
E-mail addresses: cdhan@uakron.edu (C.D. Han), jkkim@postech.ac.kr (J.K. Kim).

0032-3861/$ – see front matter © 2009 Elsevier Ltd. All rights reserved.
doi:10.1016/j.polymer.2009.03.018

From the point of view of obtaining markedly improved physical/mechanical properties of nanocomposites, exfoliation is preferred to intercalation. In order to obtain exfoliated organoclay nanocomposites, there needs to be compatibility between the surface of an organoclay and the polymer matrix. This can be achieved by matching the chemical affinity between the surfactant of an organoclay and the polymer matrix, such that specific interactions can exist. The types of specific interactions that can provide compatibility, as in the preparation of polymer blends, include hydrogen bonding, ion–ion interaction, ion–dipole interaction, the formation of electron donor–acceptor complexes, etc.

In this regard, block copolymers have greater flexibility compared to homopolymers and random copolymers in that one of the blocks can be modified with a functional group(s), such that the functionalized block can be compatible with the surfactant residing at the surface of an organoclay. Indeed, such an approach was taken by Han and coworkers [2–4] who observed highly dispersed (nearly exfoliated) organoclay nanocomposites based on functionalized block copolymers. Here we use the word "exfoliation" in *qualitative* terms, because "perfect (i.e., ideal) exfoliation" of the aggregates of natural clay and organoclay is very difficult, if not impossible, to achieve practically.

Other research groups [5,6] also reported on exfoliated nanocomposites based on block copolymers. Specifically, Ha et al. [5] first attached end-functionalized polystyrene (PS) chains to the organoclay surface either by grafting or polymerizing from the clay surface to form tethered PS chains. Then, the PS chains covered with clay were mixed, via solution blending, with a commercial polystyrene-*block*-polybutadiene-*block*-polystyrene (SBS) copolymer (Vector 4461-D, Dexco Polymers). They reported that the nanocomposite displayed exfoliated morphology. The rationale behind their approach was that the functionalized PS covered with clay layers would mix well, during solution blending, with the PS microdomains of the SBS triblock copolymer, giving rise to a well-dispersed nanocomposite. Di and Sogah [6] conducted simultaneous living free radical polymerization of styrene and anionic ring-opening polymerization of ε-caprolactone in the presence of a silicate-anchored bifunctional initiator, and obtained nanocomposites based on polystyrene-*block*-poly(ε-caprolactone) copolymer. They reported that their nanocomposite displayed exfoliated morphology.

In contrast, only intercalation of the aggregates of layered silicates was found when a block copolymer without functional group was mixed with an organoclay to obtain nanocomposites. The block copolymers employed in those studies included polystyrene-*block*-polyisoprene (SI diblock) copolymer [7,8], polystyrene-*block*-poly(ethylene-*co*-1-butene) (SEB diblock) copolymer [9,10], SIS triblock copolymer [11], SBS triblock copolymer [12], and polystyrene-*block*-poly(ethylene-*co*-1-butene)-*block*-polystyrene (SEBS triblock) copolymer [9,10,13]. An intercalated structure from those nanocomposites prepared is anticipated, because no specific interactions would be expected between SI diblock, SEB diblock, polystyrene-*block*-polyisoprene-*block*-polystyrene (SIS) triblock, SBS triblock, or SEBS triblock copolymers and an organoclay. Suffice to state, however, that with a judicious choice of the method of preparation of nanocomposites based on a functionalized block copolymer, a block copolymer mixed with a functionalized homopolymer containing silicate layers or in situ polymerization of a block copolymer in the presence of silicate layers, block copolymers can offer a promising future in the preparation of novel materials, as described in a recent review paper by Bockstaller et al. [14].

When preparing organoclay nanocomposites, one does not necessarily have to modify the chemical structure of a block copolymer if one of the blocks contains functionality. To illustrate the point, very recently we synthesized a series of polystyrene-*block*-poly(2-vinylpyridine) (S2VP diblock) copolymers with various block length ratios and then used them to prepare organoclay nanocomposites. One of the motivations of this study was to investigate the effect, if any, of the block length ratio of S2VP diblock copolymer on the dispersion characteristics of organoclay aggregates in nanocomposites. We indeed have found that the block length ratio of S2VP diblock copolymer played a significant role in determining the extent of dispersion of organoclay aggregates in nanocomposites. Interestingly, we have found that the S2VP diblock copolymer having poly(2-vinylpyridine) (P2VP) block below a certain critical level exfoliated organoclay aggregates irrespective of the differences in chemical structure of the surfactant residing at the surface of an organoclay, as long as it had an alkyl quaternary ammonium salt, giving rise to positively charged N^+ ion. We hypothesized that the experimentally observed exfoliation of those organoclay nanocomposites based on S2VP diblock copolymer might be attributable to the presence of ion–dipole interactions between the positively charged N^+ ion in the surfactant residing at the surface of the organoclay and the dipoles in the P2VP block of S2VP diblock copolymers.

In order to test the above hypothesis, we conducted solid-state nuclear magnetic resonance (NMR) spectroscopy to obtain information on ion–dipole interactions between the positively charged N^+ ion in the surfactant residing at the surface of organoclay and the dipoles in the P2VP block of S2VP diblock copolymers. Indeed, not only did we confirm the presence of ion–dipole interactions in the organoclay nanocomposites based on P2VP-containing block copolymers, but we are able to explain the reasons why the block length ratio of S2VP diblock copolymer in the organoclay nanocomposites played a significant role in determining the extent of dispersion of organoclay aggregates in these nanocomposites. To our knowledge, no investigation on ion–dipole interactions in organoclay nanocomposites has ever been reported in the literature. In this paper we report the highlights of our findings.

2. Experimental

2.1. Synthesis and characterization of polystyrene-block-poly-(2-vinylpyridine) copolymers

We synthesized, via sequential anionic polymerization, three S2VP diblock copolymers with different block length ratios, but having approximately the same molecular weight. The synthesis procedures employed for S2VP diblock copolymers are essentially the same as the standard synthesis procedures for SI diblock copolymers, which are well documented in the literature. Briefly stated, styrene monomer was first polymerized using tetrahydrofuran (THF) as solvent and *sec*-butyllithium as initiator, and then 2-vinylpyridine monomer was polymerized sequentially to the living end of the polystyrene block, yielding S2VP diblock copolymer. The block composition of the copolymers synthesized was determined using ^{1}H nuclear magnetic resonance (NMR) spectroscopy and the molecular weight was determined against polystyrene standards using gel permeation chromatography (GPC). Table 1 gives a summary of the molecular characteristics of the S2VP diblock copolymers synthesized in this study. For comparison, a homopolymer P2VP ($M_w = 9.7 \times 10^3$ and $M_w/M_n = 1.04$) was also synthesized and subsequently it was used to prepare organoclay nanocomposites.

2.2. Preparation of nanocomposites

To prepare the nanocomposites we employed a natural clay (montmorillonite MMT, Southern Clay Products), and four different organoclays: Cloisite 30B®, Cloisite 10A®, Cloisite 15A®, and Cloisite

Table 1
Molecular characteristics of S2VP diblock polymers synthesized in this study.

Sample code	M_w[a]	M_n	W_{PS}[b] (wt%)	W_{PVP}[b] (wt%)	$T_{g,PVP}$ (°C)
S2VP-5	2.29×10^4	2.14×10^4	95	5	Disordered
S2VP-25	1.96×10^4	1.87×10^4	75	25	99.6
S2VP-56	2.41×10^4	2.13×10^4	44	56	100.0

[a] Measured against polystyrene standards using gel permeation chromatography.
[b] Determined by ^{1}H NMR spectroscopy.

25A® (Southern Clay Products). The chemical structures of the surfactants residing at the surface of each organoclay are shown in Table 2 [15]. Note that among the four organoclays employed, only Cloisite 30B® has hydroxyl groups, which was confirmed by Fourier transform infrared (FTIR) spectroscopy [16]. Also given in Table 2 is the gallery distance (d_{001} spacing) of each organoclay employed. Note in Table 2 that the N^+ ion in the chemical structure of each surfactant denotes quaternary ammonium salt, T denotes tallow consisting of 65% C18, 30% C16, and 5% C14, and HT denotes hydrogenated tallow. The amount of surfactant residing at the surface of each organoclay varies as indicated in Table 2, and 100% of the Na^+ ions in MMT have been exchanged.

According to the Technical Properties Bulletin [15] from Southern Clay Products, the amount of surfactant, dimethyl tallow bis-2-hydroxyethyl quaternary ammonium chloride (MT2EtOH), residing at the surface of Cloisite 30B® is 90 meq/100 g and the amount of surfactant, dimethyl benzyl hydrogenated tallow quaternary ammonium chloride (2M2HT), residing at the surface of Cloisite 15A® is 125 meq/100 g. We have been informed by Southern Clay Products that an extremely small amount of excess surfactant is present at the surface of Cloisite 30B®, while about 30% excess surfactant is present at the surface of Cloisite 15A®, and that excess amount of surfactant residing at the surface of Cloisite 15A® can be removed when washed with methanol.

We employed solution blending to prepare organoclay nanocomposites. Namely, a predetermined amount of natural clay or organoclay was first dispersed in THF and then the polymer was added slowly, while stirring vigorously under sonication. This was done at room temperature for 30 min, followed by slow evaporation of solvent under constant stirring for 2 days. The nanocomposites were dried completely in a vacuum oven at temperatures well above the boiling point of the solvent and also at approximately 20 °C above the glass transition temperature (T_g) of the polymer until no weight change was detected. Table 3 gives a summary of sample codes of the nanocomposites based on S2VP diblock copolymers. The amount of organoclay used was 5 wt% in all nanocomposites. Since the amount of surfactant on the surface of an organoclay varies (see Table 2), the net amount of MMT in each nanocomposite varies from 3.1 to 3.8 wt% depending on the type of organoclay: 3.1 wt% for Cloisite 15A®, 3.8 wt% for Cloisite 30B®, 3.6 wt% for Cloisite 25A®, and 3.3 wt% for Cloisite 10A®.

Table 2
Chemical structures of surfactants residing at the surface of organoclay and the mean interlayer spacing (d_{001}) of organoclays employed in this study (Based on the technical bulletin of Southern Clay Products).

Sample code	Chemical structure of surfactant (wt%)		d_{001} (nm)
Cloisite 30B®	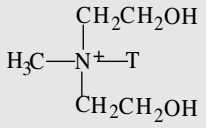	MT2EtOH (90 meq/100 g)	1.85
Cloisite 10A®	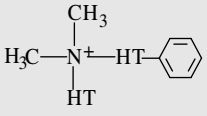	2MBHT (125 meq/100 g)	1.92
Cloisite 15A®	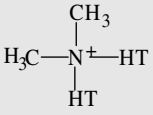	2M2HT (125 meq/100 g)	3.15
Cloisite 25A®	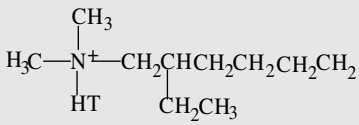	2MHTL8 (125 meq/100 g)	1.86

T in the chemical structure of surfactant denotes tallow consisting of ca. 65% C18, ca. 30% C16, and ca. 5% C14. HT in the chemical structure of surfactant denotes hydrogenated tallow consisting of ca. 65% C18%, ca. 30% C16, and ca. 5% C14. MT2EtOH is dimethyl tallow bis-2-hydroxyethyl quaternary ammonium chloride. 2MBHT is dimethyl benzyl hydrogenated tallow quaternary ammonium chloride. 2M2HT is dimethyl dehydrogenated tallow quaternary ammonium chloride. 2MHTL8 is dimethyl dehydrogenated tallow 2-ethylhexyl quaternary ammonium chloride.

2.3. X-ray diffraction (XRD)

Using a Rigaku X-ray generator operated at 40 kV and 40 mA, XRD patterns were obtained to determine the mean interlayer spacing of the (001) plane (d_{001}) for the various organoclay nanocomposites prepared in this study. The X-ray beam with a wavelength (λ) of 0.1542 nm was monochromatized to CuK_α with a graphite crystal. The range of 2θ scanning of X-ray intensity employed was 1.5–10°. Additional synchrotron XRD patterns for (S2VP-5)/MMT nanocomposite and (S2VP-56)/Cloisite 30B® nanocomposites were obtained on beamline 10C1 at the Pohang Light Source (Republic of Korea) where a double crystal Si(111) monochromator delivered monochromatic X-ray with $\lambda = 0.1594$ nm and a resolution $\Delta\lambda/\lambda \approx 0.01$ onto the sample. The reason for having conducted the additional synchrotron X-ray experiments will be given when the experimental data are presented below. The maximum difference in 2θ values calculated from the two different X-ray instruments is estimated to be about 3%.

2.4. Transmission electron microscopy (TEM)

TEM images of nanocomposite specimens stained with iodine vapor were taken at room temperature. The ultrathin sectioning

Table 3
Sample codes and compositions of nanocomposites based on S2VP diblock copolymer, which were prepared in this study.

Sample code	P2VP (wt%)
P2VP/MMT	100
P2VP/Cloisite 30B®	100
P2VP/Cloisite 15A®	100
(S2VP-5)/MMT	5
(S2VP-5)/Cloisite 30B®	5
(S2VP-5)/Cloisite 10A®	5
(S2VP-5)/Cloisite 15A®	5
(S2VP-5)/Cloisite 25A®	5
(S2VP-25)/MMT	25
(S2VP-25)/Cloisite 30B®	25
(S2VP-25)/Cloisite 15A®	25
(S2VP-56)/MMT	56
(S2VP-56)/Cloisite 30B®	56
(S2VP-56)/Cloisite 15A®	56

(50–70 nm) was performed via ultra-microtomy at room temperature for nanocomposite specimens, using a diamond knife on the Reichert Ultracut S low-temperature sectioning system. A transmission electron microscope (JEM1200EX II, JEOL) operated at 120 kV was used to record TEM images.

2.5. Small-angle X-ray scattering (SAXS)

In this study, synchrotron SAXS measurements were performed on beamline 4C1 at the Pohang Light Source (Republic of Korea), where W/B4C double multilayer monochromator delivered monochromatic X-rays with a wavelength (λ) of 0.1608 nm and a resolution $\Delta\lambda/\lambda \approx 0.01$ onto the sample. A two-dimensional CCD camera (Princeton Instruments, SCX-TE/CCD-1242) was used to collect the scattered X-rays. For the SAXS experiments, S2VP diblock copolymer samples were first annealed at 160 °C for 48 h under vacuum. The sample thickness was 1 mm.

2.6. Solid-state nuclear magnetic resonance (NMR) spectroscopy

It is well established that the proton spin-lattice relaxation time in the rotating frame ($T_{1\rho H}$) can be a sensitive measure of the extent of interactions between two components on a molecular level [17–22]. However, there is insufficient resolution in a solid-state ^{1}H spectrum to measure this directly for each component. On the other hand, there is sufficient resolution in ^{13}C spectra to resolve the components, but ^{13}C relaxation rates reflect individual environments rather than domain structure. However, if we insert a ^{1}H spin locking period before cross polarization, spectra are obtained resulting from polarization transfer from ^{1}H to ^{13}C and provide a signal where the chemical shift of the ^{13}C allows us to monitor individual structure components, while the variations in the ^{13}C signal intensities versus proton spin lock (SL) times reflect ^{1}H relaxation in the rotating frame.

The purpose of the present solid-state NMR study was to obtain *quantitative* information on ion–dipole interactions, hypothesized above, in the nanocomposites based on S2VP diblock copolymer. In this study, solid-state NMR spectra were acquired at room temperature on a Varian Inova 200 NMR spectrometer, operating at 200 MHz for ^{1}H and 50 MHz for ^{13}C. Using the pulse sequences schematically shown in Fig. 1, we measured ^{1}H–^{13}C cross polarization time (T_{CH}) which is sensitive to C–H internuclear distance and mobilities of the C–H internuclear vector. $T_{1\rho H}$ can be obtained by employing a variable contact time (CT) in the standard cross polarization and magic-angle spinning (CP/MAS) pulse sequence (see Fig. 1b) [18,22]. However, in this study, a more accurate determination of $T_{1\rho H}$ was obtained by the addition of a variable SL pulse inserted between the initial 90° pulse and a fixed optimal contact time (see Fig. 1a). Samples were spun in a Doty 7 mm magic-angle spinning (MAS) probe at a spinning speed of 5 kHz. ^{13}C chemical shifts (δ) were referenced by using hexamethylbenzene (methyl resonance at $\delta = 17.35$ ppm) as an external reference. For further details about the experimental procedures for performing the measurements the reader is referred to the literature [17,22].

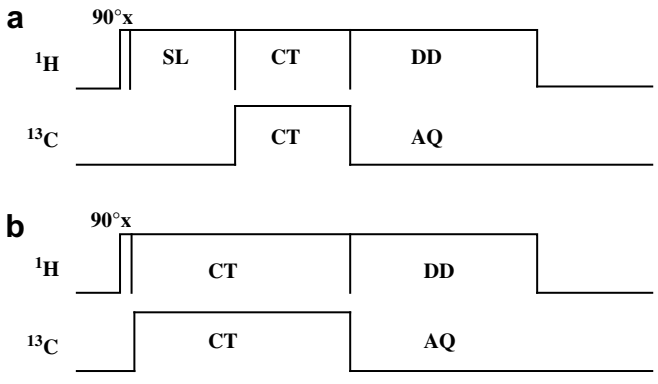

Fig. 1. Schematic of the pulse sequences used to obtain: (a) $T_{1\rho H}$, and (b) variable contact time data. In (a), a ^{1}H ($90°x$) is followed by a proton spin lock period during which $T_{1\rho H}$ relaxation occurs; the diminished ^{1}H signal is transferred to ^{13}C via a Hartman–Hahn cross polarization process during the contact time, CT, followed by detection of the ^{13}C signal during the acquisition time, AQ, with simultaneous ^{1}H dipolar decoupling, DD. In (b), the contact time, CT, is varied so that the detected ^{13}C signal intensity is altered by decay according to ^{1}H $T_{1\rho}$ and buildup of magnetization according to T_{CH}; the remainder of the sequence functions as in (a).

In all measurements data were collected with a spectral window of 20 kHz, acquisition time of 0.0256 s, and continuous wave proton dipolar decoupling during the acquisition time (using a decoupler field strength of 50 kHz). In the $T_{1\rho H}$ relaxation experiments, 200 transients were averaged for each of the $T_{1\rho H}$ relaxation spectra. Fifteen spectra were obtained with SL times ranging from 0.02 to 30 ms, with a field of 50 kHz, and cross polarization period of 3 ms using Hartman–Hahn matching fields of 50 kHz.

For the variable contact time experiments, 400 transients were averaged for collection of each of the relaxation spectra. Fifteen spectra were obtained with contact times ranging from 0.02 to 15 ms, with Hartman–Hahn matching fields of 50 kHz. To obtain a higher signal-to-noise ratio for the *ipso* carbon on the pyridine ring of S2VP-5 block copolymer as well as (S2VP-5)/Cloisite 30B, 8800 transients were averaged for collection of each of the relaxation spectra. All the data were processed by zero filling to 4096 points and exponential weighting of the time domain signal to produce line broadening of 50 Hz before Fourier transformation was performed. Data were processed using Varian VNMR 6.1c software.

Sample (S2VP-5)/Cloisite 30B® was measured twice on different dates. The error of the relaxation time measurement was analyzed using Microsoft Excel software. Five integration areas were used for the quaternary carbon signal of the P2VP segments from sample (S2VP-5)/Cloisite 30B® to evaluate the processing errors associated with contribution of signal intensity from the adjoining intense peak of the rest of the aromatic carbons.

3. Results and discussion

3.1. Dispersion characteristics of organoclay nanocomposites based on S2VP diblock copolymer as investigated by TEM and XRD

Fig. 2 gives TEM images of the nanocomposites based on S2VP diblock copolymer with different organoclays and MMT. The following observations can be made from Fig. 2. The dispersion characteristics of the MMT aggregates in the matrix of all three block copolymers (S2VP-5 containing 5 wt% P2VP block, S2VP-25 containing 25 wt% P2VP block, and S2VP-56 containing 56 wt% P2VP block) are very poor (Fig. 2a,d, and g). This is because no attractive interaction is expected between the surface of MMT and the pyridine rings in the P2VP block of the S2VP diblock copolymers. On the other hand, we observe from Fig. 2 that the dispersion characteristics of the aggregates of Cloisite 30B® and Cloisite 15A® in the matrix of S2VP-5 are very good, despite the fact that the chemical structures of the surfactant residing at the surface of both organoclays are different (see Table 2). We also observed very high degree of dispersion characteristics of the aggregates of Cloisite 10A® and Cloisite 25A® in the matrix of S2VP-5. However, due to the space limitation, those results are not presented here. Below, we will provide an explanation on this somewhat expected experimental observation. It should be mentioned that in general,

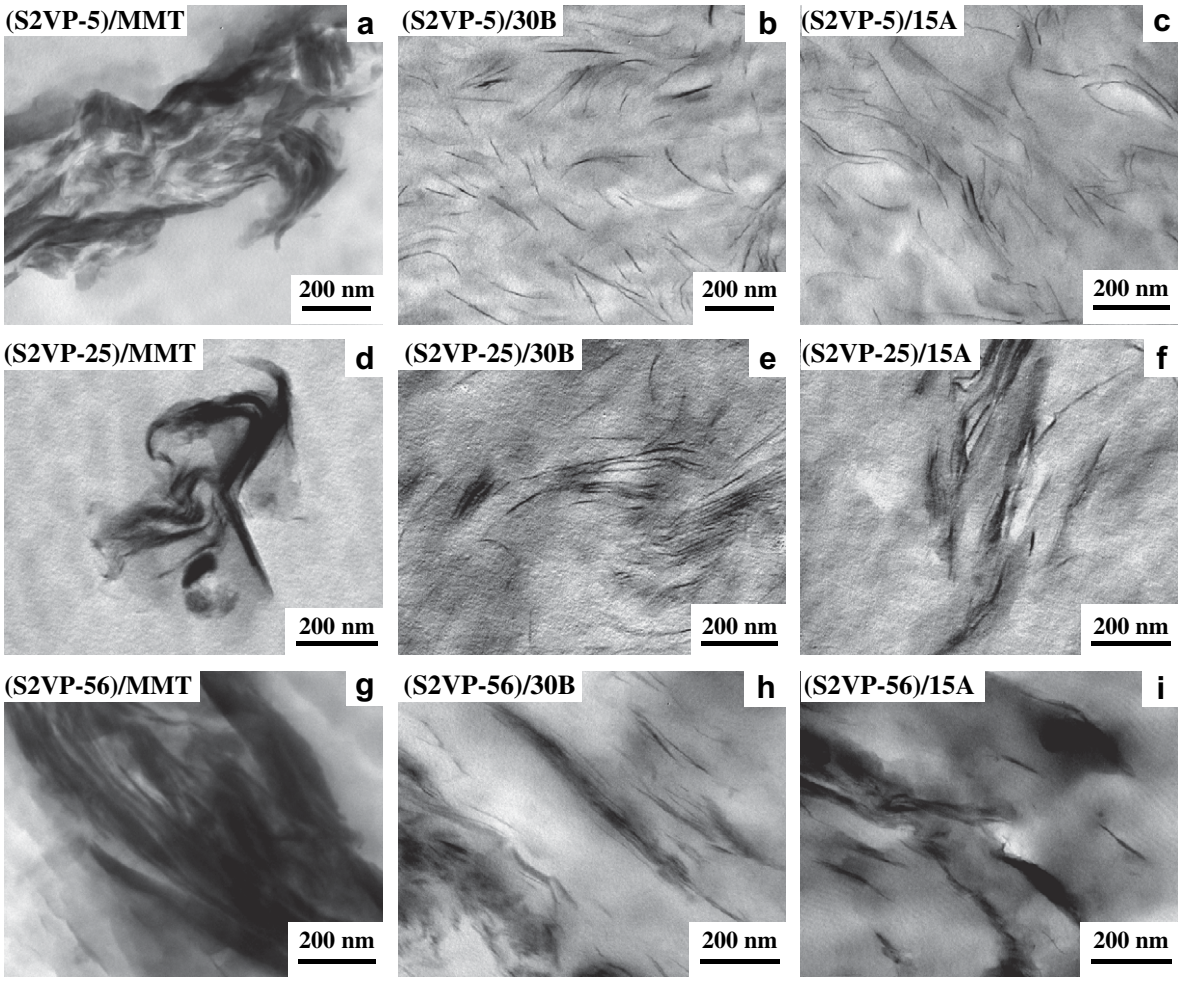

Fig. 2. TEM images of nanocomposites based on S2VP-5: (a) (S2VP-5)/MMT, (b) (S2VP-5)/Cloisite 30B®, (c) (S2VP-5)/Cloisite 15A®, (d) (S2VP-25)/MMT, (e) (S2VP-25)/Cloisite 30B®, (f) (S2VP-25)/Cloisite 15A®, (g) (S2VP-56)/MMT, (h) (S2VP-56)/Cloisite 30B®, and (i) (S2VP-56)/Cloisite 15A®. Specimens were not stained.

the chemical structure of the surfactant residing at the surface of an organoclay has a profound influence on the dispersion characteristics of organoclay nanocomposites [23,24]. It is interesting to observe that the dispersion characteristics of the aggregates of Cloisite 30B® and Cloisite 15A® become progressively poorer as the weight fraction of P2VP block in an S2VP diblock copolymer increases from 5 wt% (see Fig. 2b for (S2VP-5)/Cloisite 30B® nanocomposite and Fig. 2c for (S2VP-5)/Cloisite 15A® nanocomposite) to 25 wt% (see Fig. 2e for (S2VP-25)/Cloisite 30B® nanocomposite and Fig. 2f for (S2VP-25)/Cloisite 15A® nanocomposite) and to 56 wt% (see Fig. 2h for (S2VP-56)/Cloisite 30B® nanocomposite and Fig. 2i for (S2VP-56)/Cloisite 15A® nanocomposite). Below, we will offer an explanation on the origin of the different dispersion characteristics observed in the organoclay nanocomposites as affected by the amount of P2VP block in an S2VP diblock copolymer.

Fig. 3 shows XRD patterns of nanocomposites based on S2VP with various block copolymer compositions, each having two different organoclays. Also shown in Fig. 3 are, for comparison, XRD patterns of nanocomposites having MMT. In Fig. 3a we observe that the XRD pattern (curve 1) of MMT shows a conspicuous reflection peak for at $2\theta \approx 7.5^\circ$ which gives a d-spacing of 1.11 nm and the XRD pattern (curve 2) of (S2VP-5)/MMT nanocomposite exhibits a somewhat broader reflection peak at $2\theta \approx 7.5$–8.0° obtained using a synchrotron X-ray facility, corresponding to a d-spacing of about 1 nm. That is, the d-spacing (the gallery distance) of MMT in the matrix of S2VP-5 is very close to the gallery distance of 1.1 nm for pristine MMT. This observation suggests that the dispersion characteristics of the aggregates of MMT in (S2VP-5)/MMT nanocomposite are very poor, consistent with the observations made from the TEM image given in Fig. 2a. Namely, little or no attractive interaction took place between MMT and the pyridine rings in the P2VP block of S2VP-5. When a Rigaku X-ray generator was used, the XRD pattern of (S2VP-5)/MMT nanocomposite did not exhibit any discernible reflection peak and the XRD pattern of (S2VP-56)/Cloisite 30B nanocomposite did not exhibit a refection peak at $2\theta \approx 4.1^\circ$. These observations indicate that the XRD patterns (d-spacing) of nanocomposites based on natural clay or organoclay can often give rise to misleading information on the dispersion characteristics of nanocomposites. For instance, it is quite possible that a small number of well-dispersed silicate platelets can obscure the d-spacing in XRD patterns. Further, the intensity of a reflection peak (d-spacing) can easily be changed depending on the methods of sample preparation employed. Thin composite films or specimens prepared under high compression tend to orient the silicate platelets in the plane direction, which may then change significantly the intensity of signal, as compared with the specimen that was prepared in such a way that it has random distribution of platelets. Thus, we conclude that often XRD patterns alone are not sufficient to make definitive conclusions about the dispersion characteristics of nanocomposites. In this regard, it is fair to state

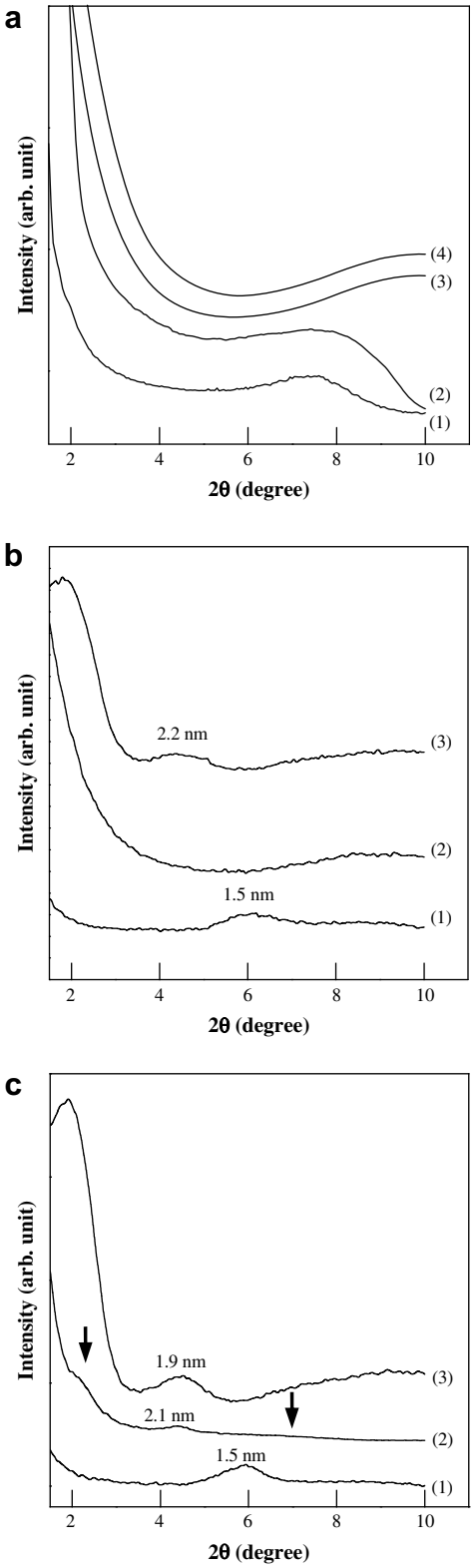

Fig. 3. XRD patterns for nanocomposites: (a) based on S2VP-5: (1) pristine MMT (2) (S2VP-5)/MMT, (3) (S2VP-5)/Cloisite 30B®, and (4) (S2VP-5)/Cloisite 15A®. (b) based on S2VP-25: (1) (S2VP-25)/MMT, (2) (S2VP-25)/Cloisite 30B®, (3) (S2VP-25)/Cloisite 15A®; (c) based on S2VP-56: (1) (S2VP-56)/MMT, (2) (S2VP-56)/Cloisite 30B®, and (3) (S2VP-56)/Cloisite 15A®. Note that the XRD patterns for (S2VP-5)/MMT and (S2VP-56)/Cloisite 30B® nanocomposites were obtained using a synchrotron X-ray facility and the XRD patterns for other nanocomposites were obtained using a Rigaku X-ray generator.

that TEM images are essential for determining the dispersion characteristics of nanocomposites.

On the other hand, in the XRD patterns given in Fig. 3a(3) and a(4) we do not observe a discernible reflection peak at 2θ angles ranging from 1.5 to 10° for the organoclay nanocomposites based on Cloisite 30B® or Cloisite 15A®, despite the fact that the chemical structures of surfactant residing at the surface of the organoclays (Cloisite 30B® and Cloisite 15A®) are different (see Table 2). In general, the absence of a discernible reflection peak in XRD patterns signifies good dispersion of the organoclay in a polymer matrix. Thus, we can conclude that the dispersion characteristics of both organoclay nanocomposites based on S2VP-5 would be very good, consistent with the observations made from the TEM images given in Fig. 2.

We observe from Fig. 3b(1) that the XRD pattern of (S2VP-25)/MMT nanocomposite shows a conspicuous reflection peak at $2\theta \approx 6°$ (d-spacing = 1.5 nm), suggesting poor dispersion of MMT aggregates in the S2VP-25 matrix, although some MMT aggregates might have been intercalated. Interestingly, in Fig. 3b(2) we observe a very broad reflection peak at $2\theta \approx 8.4°$ in the XRD pattern of (S2VP-25)/Cloisite 30B® nanocomposite. This broad peak was not observed in (S2VP-5)/Cloisite 30B® nanocomposite (see Fig. 3a(3)). This observation seems to indicate that small amounts of Cloisite 30B® aggregates in the S2VP-25 matrix might have been poorly dispersed, although most of the Cloisite 30B® aggregates are well dispersed. Thus, the overall dispersion characteristics of Cloisite 30B® in the S2VP-25 matrix would be slightly poorer than those in the S2VP-5 matrix, consistent with the TEM images (compare Fig. 2b with Fig. 2e). From the XRD pattern given in Fig. 3b(3) we observe a reflection peak at $2\theta \approx 1.8°$ (d-spacing = 5.0 nm) and a conspicuous reflection peak at $2\theta \approx 4.1°$ (d-spacing = 2.2 nm) in (S2VP-25)/Cloisite 15A® nanocomposite. Since the gallery distance of pristine Cloisite 15A® is 3.15 nm (which will be shown below), the overall dispersion characteristics of Cloisite 15A® in the S2VP-25 matrix would be poorer than those in the S2VP-5 matrix, consistent with the TEM images (compare Fig. 2c with Fig. 2f).

From Fig. 3c(1) we observe that the XRD pattern of (S2VP-56)/MMT nanocomposite shows a conspicuous reflection peak at $2\theta \approx 6°$ (d-spacing = 1.5 nm), very similar to that of (S2VP-25)/MMT nanocomposite (see Fig. 3b(1)), suggesting again poor dispersion of MMT aggregates in the S2VP-56 matrix, although some intercalations might have taken place. From Fig. 3c(2) we observe that the (S2VP-56)/Cloisite 30B® nanocomposite has a small distinct reflection peak at $2\theta \approx 4.3°$ (d-spacing = 2.1 nm) and two weak reflection peaks pointed by arrows $2\theta \approx 2.15°$ (d-spacing = 4.2 nm) and 7.3° (d-spacing = 1.24 nm). Since the gallery distance of pristine Cloisite 30B® is 1.85 nm (which will be shown below), it seems reasonable to speculate that the (S2VP-56)/Cloisite 30B® nanocomposite has aggregates of Cloisite 30B® with varying gallery distances. Thus, it seems reasonable to speculate that some of the Cloisite 30B® aggregates might have been dispersed well, while others might have been intercalated in the matrix of S2VP-56. However, since two reflection peaks for (S2VP-56)/Cloisite 30B® nanocomposite are discernible at $2\theta = 2.15°$ and 4.3°, the dispersion characteristics of Cloisite 30B® aggregates in the S2VP-56 matrix would be poorer compared with those in the S2VP-25 matrix, consistent with the TEM images (see Fig. 2e and h). From Fig. 3c(3) we observe that the XRD patterns of (S2VP-56)/Cloisite 15A® nanocomposite have conspicuous reflection peaks at $2\theta \approx 1.9°$ and 4.4°, suggesting poor dispersion of Cloisite 15A® in the matrix of S2VP-56, although some intercalations of Cloisite 15A® aggregates might have taken place.

On the basis of the observations made above from Figs. 2 and 3, it is clear that the dispersion characteristics of organoclay nanocomposites based on an S2VP diblock copolymer become progressively poorer as the amount of P2VP block increases from

5 wt% in S2VP-5 to 25 wt% in S2VP-25 and to 56 wt% in S2VP-56. This is attributed to the fact that the extent of self-association of pyridine rings in the P2VP block of an S2VP diblock copolymer becomes stronger as the amount of P2VP block increases, hindering interactions between the pyridine rings in the P2VP block and the surfactant (MT2EtOH or 2M2HT) residing at the surface of Cloisite 30B® or Cloisite 15A® and thus giving rise to poor dispersion (at best intercalation) of organoclay nanocomposites. Earlier, Han and coworkers [4] have made similar observations.

The above observation can best be illustrated with the TEM images shown in Fig. 4 and from the XRD patterns shown in Fig. 5 for nanocomposites based on neat P2VP with MMT, Cloisite 30B® or Cloisite 15A®. For comparison, also given in Fig. 5 are XRD patterns of MMT, Cloisite 30B®, and Cloisite 15A®. It is clearly seen from Figs. 4 and 5 that although there are numerous pyridine groups in neat P2VP that can have attractive interactions with a surfactant

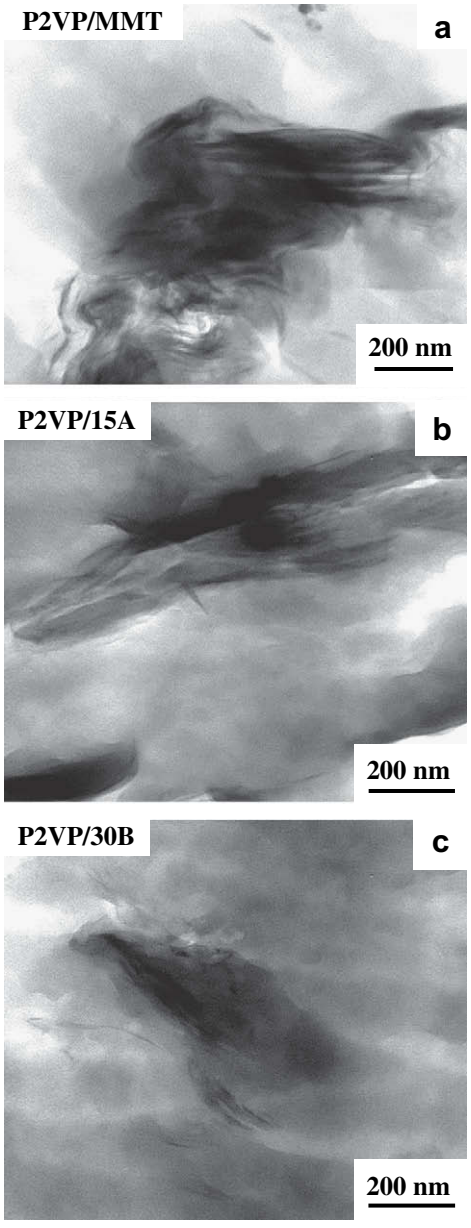

Fig. 4. TEM images of nanocomposites based on P2VP: (a) P2VP/MMT, (b) P2VP/Cloisite 15A®, and (c) P2VP/Cloisite 30B®. Specimens were not stained.

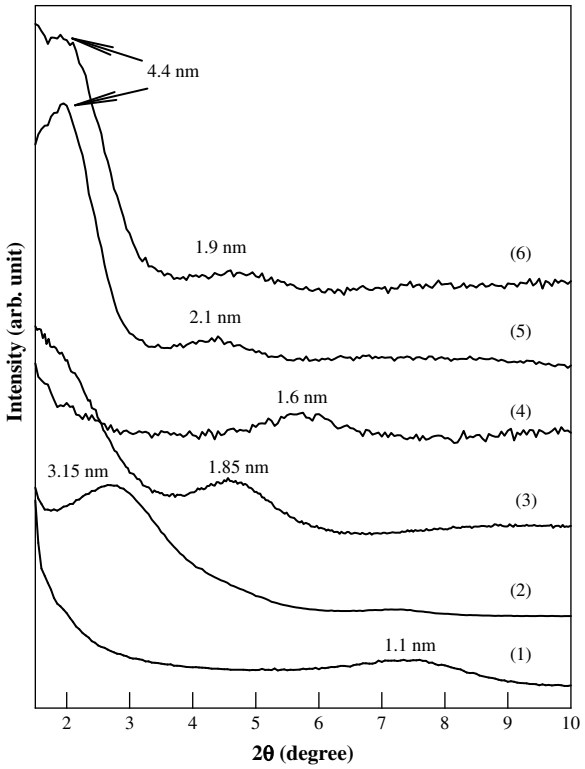

Fig. 5. XRD patterns for nanocomposites based on P2VP: (1) MMT, (2) Cloisite 15A®, (3) Cloisite 30B®, (4) P2VP/MMT, (5) P2VP/Cloisite 15A®, and (6) P2VP/Cloisite 30B®.

(MT2EtOH or 2M2HT) residing at the surface of Cloisite 30B® or Cloisite 15®, the dispersion characteristics of P2VP/Cloisite 30B® and P2VP/Cloisite 15A® nanocomposites are as poor as the dispersion characteristics of P2VP/MMT nanocomposite although some intercalations of organoclay aggregates might have taken place. This is because the pyridine rings in neat P2VP form self-association and thus little or no intermolecular interactions take place with a surfactant residing at the surface of an organoclay (Cloisite 30B® or Cloisite 15A®). This observation reinforces our view that the strong self-association within the molecules of P2VP block in S2VP-25 and S2VP-56, respectively, has given rise to poor dispersion of the respective organoclay nanocomposites. In other words, a very high degree of exfoliation observed in the (S2VP-5)/Cloisite 30B® and (S2VP-5)/Cloisite 15A® nanocomposites has originated from the presence of a very weak, if any, self-association of the pyridine rings in the P2VP block in S2VP-5.

It should be mentioned that the molecular weight (M_w) of neat P2VP employed for preparing the nanocomposites with MMT, Cloisite 30B®, or Cloisite 15A® is 10,000, while the M_w of P2VP block in S2VP-5 is 1145, the M_w of P2VP in S2VP-25 is 4900, and the M_w of P2VP block in S2VP-56 is 13,500. We did not prepare organoclay nanocomposites based on a neat P2VP having an M_w which is comparable to that of P2VP block in S2VP-5, because such a low molecular weight (about 10 repeat units) P2VP can be regarded as being essentially an oligomer, but not a polymer. In other words, any attempt to use such a low molecular weight neat P2VP to prepare an organoclay nanocomposite is little different from mixing an organoclay with a polar solvent. The experimental observation that the extent of dispersion of the organoclay nanocomposite based on neat P2VP having $M_w = 10{,}000$, indicated by Figs. 4 and 5, is as poor as that of the nanocomposites based on S2VP-25 having P2VP block with $M_w = 4900$ and based on S2VP-56 having PVP block with $M_w = 13{,}500$, suggests that the molecular

weight of P2VP block in an S2VP diblock copolymer has played little roles in determining the effectiveness of exfoliating the organoclay nanocomposites based on Cloisite 30B® or Cloisite 15A®. We wish to point out that the mobility of P2VP block in an S2VP diblock copolymer would be lower than that of neat P2VP in THF, because the P2VP block in an S2VP diblock copolymer is covalently bonded to the PS block. Therefore, a direct comparison of molecular mobility between the P2VP block in an S2VP diblock copolymer and neat P2VP is not warranted.

A chemical modification of natural clay, which is hydrophilic, not only increases its gallery distance, but also the surfactant used to chemically modify the surface of natural clay makes the organoclay more organophilic and hydrophobic. Note that the functional group(s) in a surfactant residing at the surface of an organoclay can have attractive interactions with the functional group(s) in a polymer chain. For instance, the hydroxyl groups in the surfactant MT2EtOH residing at the surface of Cloisite 30B® can potentially form hydrogen bonds with the nitrogen atom on the pyridine rings in the P2VP block of S2VP block copolymers. Interestingly, however, in Fig. 2 we also observe a very high degree of dispersion of Cloisite 15A® aggregates in the nanocomposite based on S2VP-5 although the surfactant 2M2HT residing at the surface of Cloisite 15A® does not have a hydroxyl group. This observation leads us to speculate that there might have existed ion–dipole interactions between the positively charged N^+ ion in the surfactant 2M2HT residing at the surface of Cloisite 15A® (or in the surfactant MT2EtOH residing at the surface of Cloisite 30B®) and the pyridine rings in the P2VP block of S2VP diblock copolymer. That is, the TEM images shown in Fig. 2b and c indicate that the aggregates of both organoclays (Cloisite 30B® and Cloisite 15A®) are dispersed equally well in the S2VP-5 matrix, irrespective of the differences in chemical structures of the surfactants residing at the surface of the respective organoclay as long as the surfactants have positively charged N^+ ions. Thus, we hypothesize that the highly dispersed organoclay nanocomposites based on S2VP-5 with Cloisite 30B® or Cloisite 15A® are attributable to the presence of ion–dipole interactions.

3.2. Morphology of organoclay nanocomposites based on S2VP diblock copolymer

Fig. 6 shows TEM images of (S2VP-25)/Cloisite 30B® and (S2VP-56)/Cloisite 30B® nanocomposites after staining with osmium tetroxide. It is clearly seen from Fig. 6 that S2VP-25 in the (S2VP-25)/Cloisite 30B® nanocomposite remains as a disordered block copolymer, while S2VP-56 in the (S2VP-56)/Cloisite 30B® nanocomposite has lamellar microdomains. In Fig. 2 we already have confirmed that the aggregates of Cloisite 30B® or Cloisite 15A® are not well dispersed in S2VP-56, which is indirect evidence that ion–dipole interactions between the positively charged N^+ ion in the surfactant MT2EtOH residing at the surface of Cloisite 30B® (or in the surfactant 2M2HT residing at the surface of Cloisite 15A®) and the pyridine rings in the P2VP block of S2VP-56 might be very weak owing to the very strong self-association of pyridine rings in the P2VP block of S2VP-56.

Fig. 7 shows SAXS profiles of (a) neat S2VP-5 and (S2VP-5)/Cloisite 30B® nanocomposite, (b) neat S2VP-25 and (S2VP-25)/Cloisite 30B® nanocomposite, and (c) neat S2VP-56 and (S2VP-56)/Cloisite 30B® nanocomposite. It is seen in Fig. 7 that the two neat diblock copolymers, S2VP-5 and S2VP-25, are in the disordered state and that S2VP-56 is a lamella-forming diblock copolymer. It should be mentioned that the SAXS profiles of disordered block copolymers exhibit a broad scattering peak, while homopolymers do not, due to the "correlation hole" effect (namely, due to the existence of concentration (or composition) fluctuations of one component in the space) predicted by the Leibler theory [25].

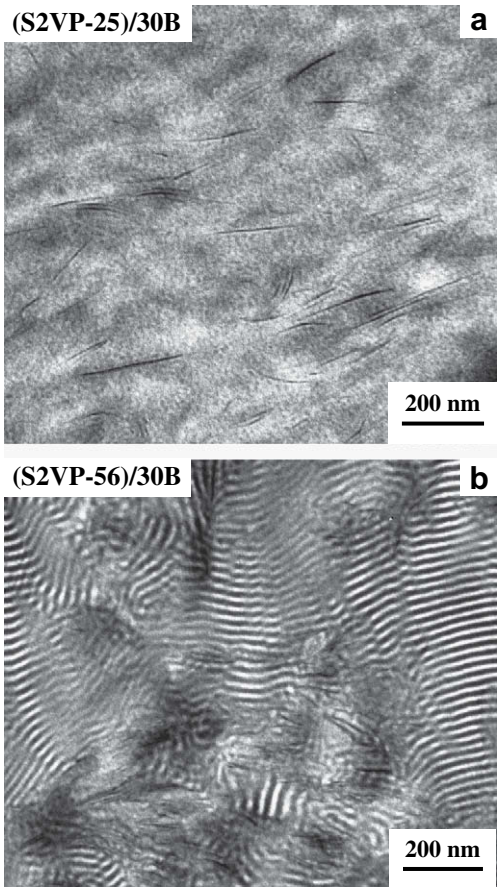

Fig. 6. TEM images of (a) (S2VP-25)/Cloisite 30B® nanocomposite and (b) (S2VP-56)/Cloisite 30B® nanocomposite, in which the specimens were stained with iodine.

However, it is very difficult to observe a broad scattering peak in the SAXS profile when a disordered block copolymer has a very small volume fraction of one component. This is precisely the reason why in the SAXS profiles of neat diblock copolymer S2VP-5 and (S2VP-5)/Cloisite 30B® nanocomposite (Fig. 7a) a broad scattering peak is not discernible. Note that S2VP-5 has only 5 wt% P2VP block. On the other hand, in Fig. 7b we observe a broad scattering peak in the SAXS profile of neat S2VP-25, because the amount of P2VP block is sufficiently large (25 wt%). Notice further from Fig. 7c that the SAXS profiles of neat diblock copolymer S2VP-56 and (S2VP-56)/Cloisite 30B® nanocomposite exhibit a very strong scattering peak, signature of an ordered state of S2VP-56, although the reflection peak of S2VP-56 in the (S2VP-56)/Cloisite 30B® nanocomposite is not as sharp as that of neat S2VP-56. This is because in the nanocomposite the lamellar microdomains of S2VP-56 near the clay platelets were not well developed, as can be seen in Fig. 6b. In summary, the SAXS study has confirmed the conclusion drawn from TEM images.

3.3. Evidence of ion–dipole interactions in the organoclay nanocomposites based on S2VP diblock copolymer as determined by solid-state NMR spectroscopy

Above we have hypothesized that the very high degree of dispersion observed experimentally in organoclay nanocomposites based on S2VP-5 is attributable to ion–dipole interactions between the pyridine ring in the P2VP block of S2VP-5 and the positively charged N^+ ion present in the surfactant (MT2EtOH, 2MBHT, 2M2HT, or 2MHT8L) residing at the surface of organoclay (Cloisite

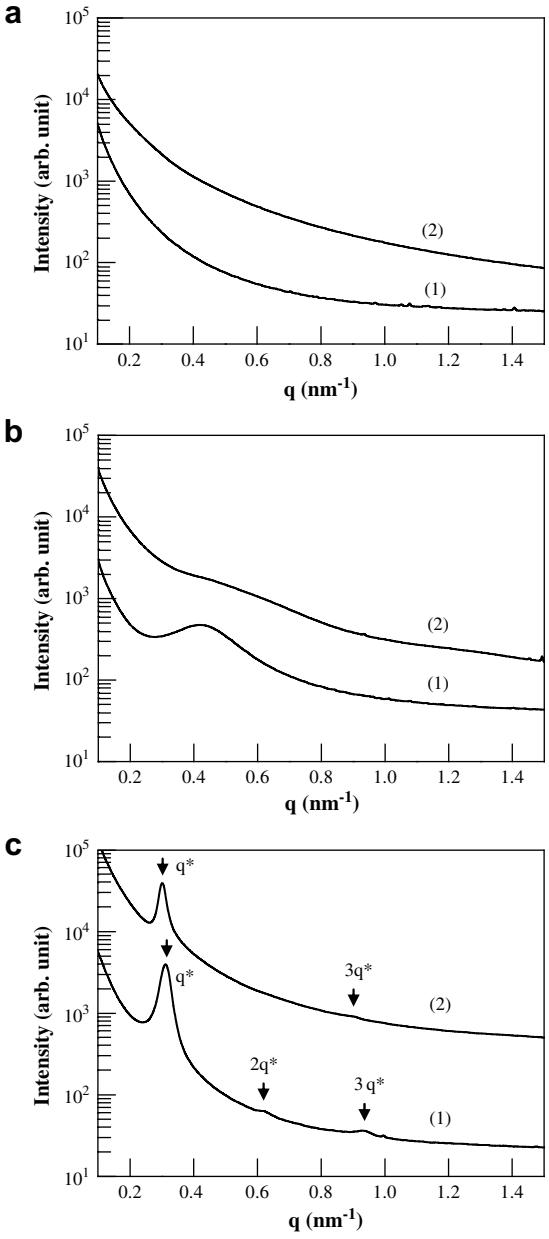

Fig. 7. SAXS profiles at 160 °C for: (a) (1) neat S2VP-5 and (2) (S2VP-5)/Cloisite 30B® nanocomposite, (b) (1) neat S2VP-25 and (2) (S2VP-25)/Cloisite 30B® nanocomposite, and (c) (1) neat S2VP-56 and (2) (S2VP-56)/Cloisite 30B® nanocomposite.

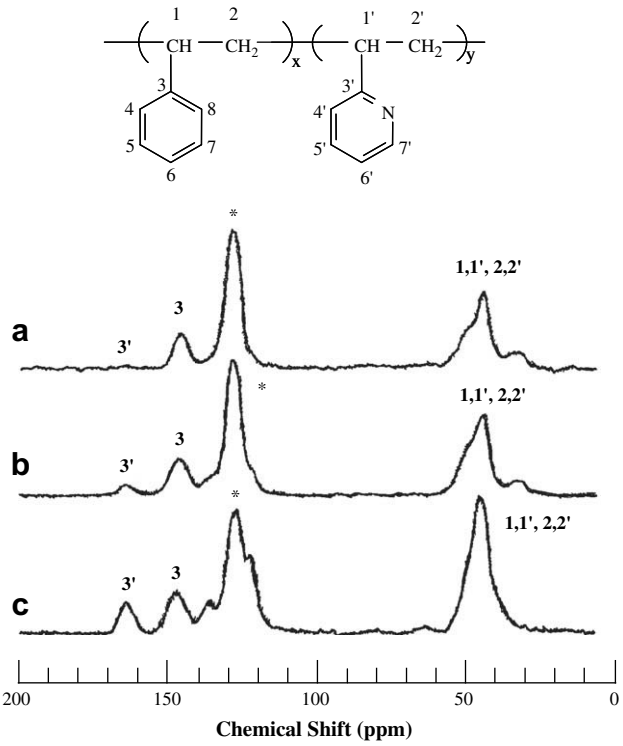

Fig. 8. ^{13}C CP/MAS spectra of (a) S2VP-5, (b) S2VP-25, and (c) S2VP-56, in which * denotes the chemical shift of the carbons at positions 4, 5, 6, 7, 8, 4′, 5′, 6′, and 7′. The intensity of carbon resonance at $\delta = 163.1$ ppm from the P2VP block in S2VP-5 is so weak that it is not easily discernible.

30B®, Cloisite 15A®, Cloisite 20A®, or Cloisite 25A®) (see Table 2). Our hypothesis was based on the premise that strong attractive interactions, via ion–dipole interactions, existed between S2VP-5 and the surfactant residing at the surface of organoclay, enhancing miscibility between the two, and thus yielded a highly dispersed organoclay nanocomposite. As a matter of fact, earlier, some research groups [26–29] reported on miscibility enhancement in binary polymer blends by ion–dipole interactions. Specifically, Hara and Eisenberg [26] reported that ion–dipole interactions enhanced miscibility in binary polymer blends consisting of poly(propylene oxide) and poly(styrene-*ran*-methacrylic acid) having 9.5 mol% lithium methacrylate. They determined that an enhancement of miscibility occurred for the blends from dynamic mechanical measurements and differential scanning calorimetry (DSC), but they did not present direct evidence of the presence of ion–dipole interactions in the blends using spectroscopic method. On the other hand, Lim et al. [29] employed FTIR spectroscopy to confirm the presence of ion–dipole interactions in blends consisting of poly(ethylene oxide) (PEO) and poly(styrene-*ran*-sodium methacrylate) (P(S-*ran*-NaMA)) copolymer, which was obtained by neutralizing poly(styrene-*ran*-methacrylic acid) copolymer with sodium hydroxide (NaOH) yielding an ionomer. In their study, Lim et al. obtained direct evidence of ion–dipole interactions between the carboxylate ion ($-COO^-$) in P(S-*ran*-NaMA) copolymer and the ether groups in PEO, and then concluded that the presence of ion–dipole interactions enhanced significantly the miscibility of PEO/P(S-*ran*-NaMA) blends as determined by FTIR spectroscopy.

Table 4
Proton $T_{1\rho H}$ data for PS, P2VP, S2VP diblock copolymers and their nanocomposites.

Sample code	$T_{1\rho H}$ (μs)						
	Peak position δ (ppm)						
	163.09	145.78	133.85	125.00	119.81	40.57	Average
Neat PS		4900		6000		5100	5300
PS/Cloisite 30B®		5800		5600		5600	5700
Neat P2VP	5900	6988		7200	6000	6500	6500
P2VP/Cloisite 30B®	640	7200		6200	6400	6200	6500
S2VP-5		5300		5700		5300	5500
(S2VP-5)/ Cloisite 30B®		5700		5900		5900	5800
S2VP-25	6900	5500		5600		5800	6100
(S2VP-25)/ Cloisite 30B®	6600	5600		5400		5300	5700
S2VP-56	5700	5900	6100	5900	6100	5500	5600
(S2VP-56)/ Cloisite 30B®	5700	5400	5900	5700		5600	5800

Here we present our experimental results showing the presence of ion–dipole interactions in the nanocomposites investigated in this study, as determined by solid-state NMR spectroscopy, thereby supporting the validity of the hypothesis made above. Fig. 8 shows the solid-state ^{13}C CP/MAS spectra of three neat S2VP diblock copolymers: (a) S2VP-5, (b) S2VP-25, and (c) S2VP-56. While the main chain (aliphatic) carbon resonances and most of the aromatic carbon resonances of both the PS and P2VP blocks overlap, a unique non-overlapping carbon resonance from the P2VP block in S2VP-56 appears at $\delta = 163.1$ ppm (see Fig. 8c), which comes from the *ipso* carbon of the pyridine ring in P2VP block. This unique signal can be used to probe the heterogeneity of the segmental motion and interaction of the P2VP block with organoclay. Values of $T_{1\rho H}$ for neat PS, neat P2VP, neat S2VP diblock copolymers and their nanocomposites were determined and they are summarized in Table 4. Due to the heterogeneous nature of neat S2VP diblock copolymers and their nanocomposites, the values of $T_{1\rho H}$ were averaged on the timescale of the spin locking periods. Therefore, only a single value of $T_{1\rho H}$ was measured.

Fig. 9 gives stacked ^{13}C CP/MAS spectra at fifteen different contact times for three nanocomposites: (a) (S2VP-5)/Cloisite 30B®, (b) (S2VP-25)/Cloisite 30B®, and (c) (S2VP-56)/Cloisite 30B®. Notice in Fig. 9a that the carbon resonance, which should come from the *ipso* carbon of the pyridine ring in P2VP block of S2VP-5 in the (S2VP-5)/Cloisite 30B® nanocomposite is weak for two reasons: (1) only 5 wt% P2VP block is present in S2VP-5 and (2) the pyridine ring in P2VP has already interacted, via ion–dipole interactions, with the N^+ ion in the surfactant 2M2EtOH residing at the surface of Cloisite 30B®. Below we will elaborate on this as to how we have analyzed the weak signal when determining values of T_{CH} in the (S2VP-5)/Cloisite 30B® nanocomposite. In order to help observe in Fig. 9a the carbon resonance that would arise from the *ipso* carbon of the pyridine ring in the P2VP block of S2VP-5, using a dotted line we have indicated a small section covering the chemical shifts ranging from 140 to 175 ppm, and then prepared Fig. 10 describing enlarged stacked ^{13}C CP/MAS spectra at twelve different contact times for the (S2VP-5)/Cloisite 30B® nanocomposite. In Fig. 10 we discern a carbon resonance at $\delta = 163.1$ ppm arising from the *ipso* carbon of the pyridine ring in the P2VP block. Notice in Fig. 10 that the carbon resonance intensity at $\delta = 163.1$ ppm increases with increasing contact time.

The dependence of the magnetization, M, as a function of the contact time t may be written as [30]

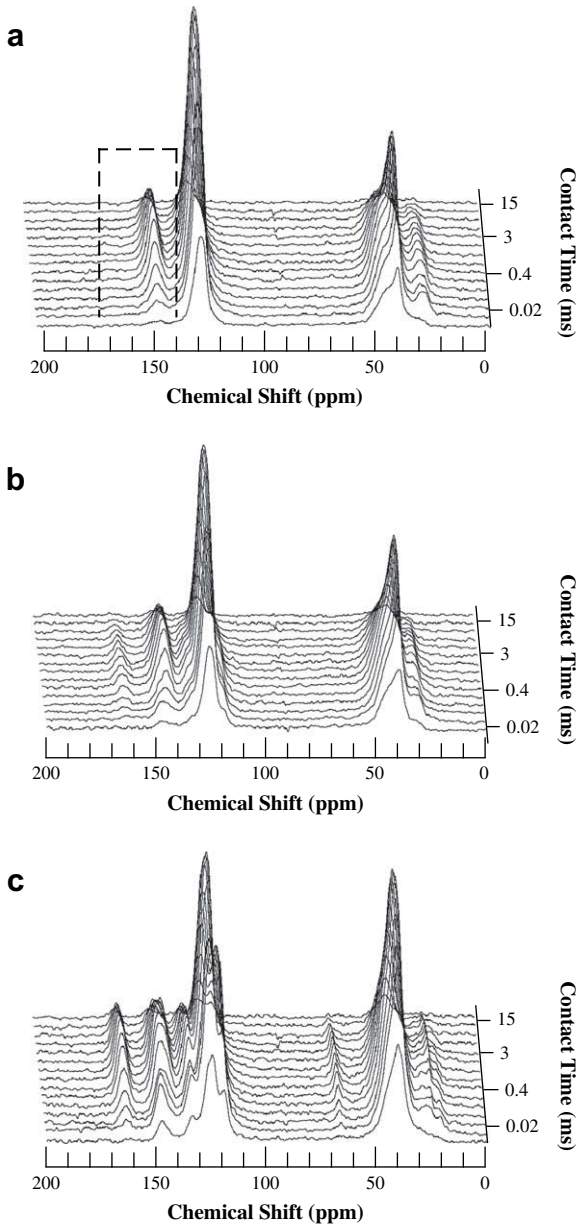

Fig. 9. Stacked ^{13}C CP/MAS spectra at 15 different contact times (ms) (0.02, 0.05, 0.1, 0.2, 0.4, 0.7, 1.0, 1.5, 2.0, 3.0, 4.0, 5.0, 7.0, 10, and 15) for: (a) (S2VP-5)/Cloisite 30B® nanocomposite, (b) (S2VP-25)/Cloisite 30B® nanocomposite, and (c) (S2VP-56)/Cloisite 30B® nanocomposites.

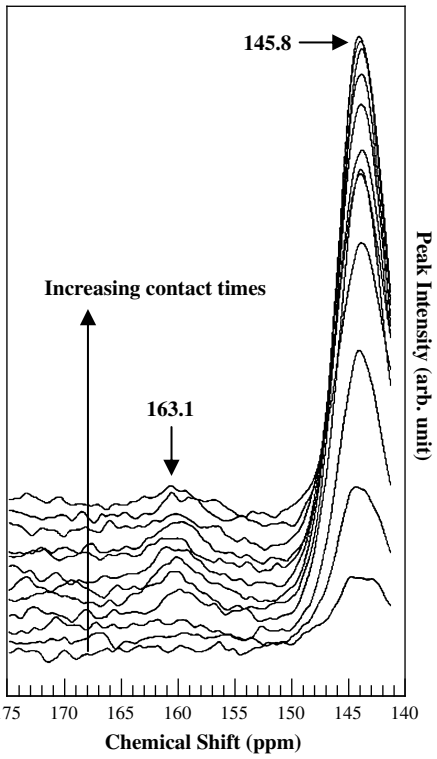

Fig. 10. Enlarged stacked ^{13}C CP/MAS spectra at $\delta = 140$–175 ppm at twelve different contact times increasing from 0.02 to 15 ms for the (S2VP-5)/Cloisite 30B® nanocomposite. Owing to the crowdedness of the spectra, values of contact times are not shown in the figure.

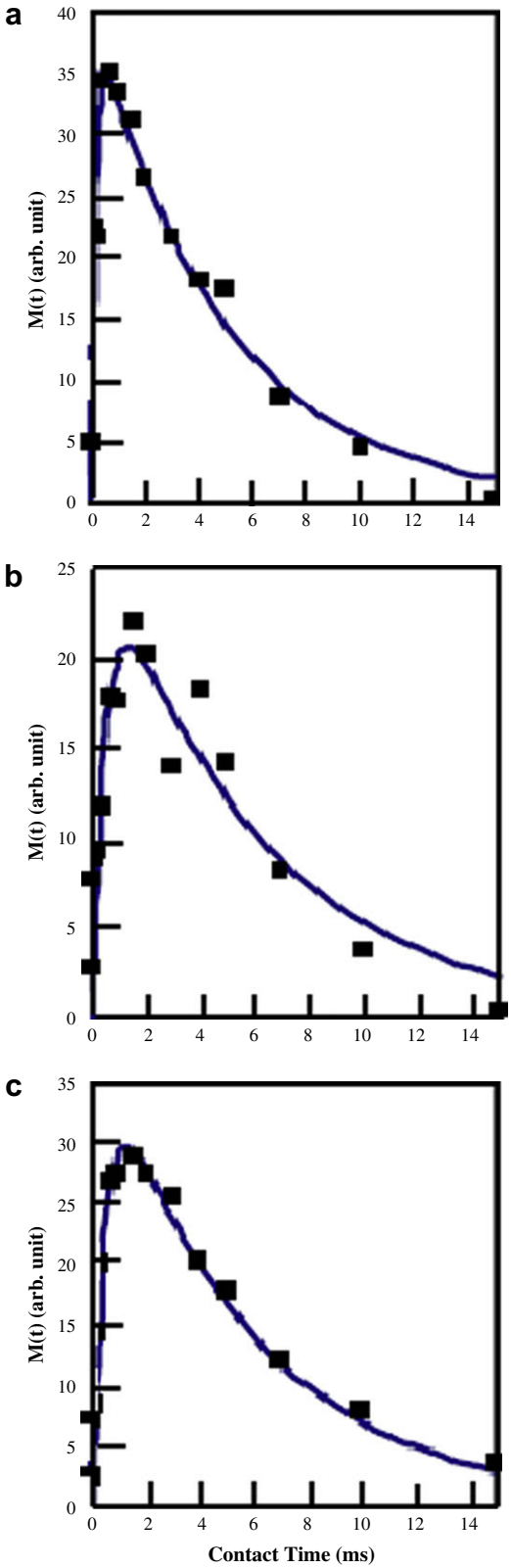

Fig. 11. Plots of $M(t)$ of ^{13}C CP/MAS spectra at $\delta = 163.1$ ppm versus contact time for three neat block copolymers: (a) S2VP-5, (b) S2VP-25, and (c) S2VP-56, in which the symbols represent experiment data and the solid lines represent the best fit from the Excel fitting procedure employed.

$$M(t) = M_0[1 - \exp(-\lambda t/T_{CH})]\exp(-t/T_{1\rho H}) \quad (1)$$

where $\lambda = 1 + (T_{CH}/T_{1\rho C}) - (T_{CH}/T_{1\rho H})$, $M(t)$ denotes the magnetization at contact time t which is proportional to the peak intensity of a particular resonance in the ^{13}C CP/MAS spectra, M_0 denotes the initial equilibrium magnetization, T_{CH} denotes the cross polarization time, $T_{1\rho C}$ denotes the carbon spin-lattice relaxation time in the rotating frame, and the $T_{1\rho H}$ denotes the proton spin-lattice relaxation time in the rotating frame.

Very often, in rigid polymeric materials, $T_{CH} << T_{1\rho C}$ and $T_{1\rho H}$, and Eq. (1) can be simplified to

$$M(t) = M_0[1 - \exp(-t/T_{CH})]\exp(-t/T_{1\rho H}) \quad (2)$$

Initially we curve-fit, with the aid of the Varian VNMR 6.1c software, the peak intensity of the $\delta = 145.8$ ppm peak from the ^{13}C CP/MAS spectra (see Fig. 9), using Eq. (2) and varying three parameters (M_0, T_{CH}, and $T_{1\rho H}$). We found that it was difficult to obtain satisfactory curve fitting with large differences between experimental and calculated curves. Thus, we decided to conduct additional proton spin lock experiments using the pulse sequence schematically shown in Fig. 1a, with the longest spin lock time of 30 ms. The average values of $T_{1\rho H}$ thus obtained for neat block copolymers and their nanocomposites are summarized in the last column of Table 4. Having these independently determined values of $T_{1\rho H}$, we made another attempt to curve-fit the data to Eq. (2) with the aid of the solver feature of Microsoft Excel software, and by varying only M_0 and T_{CH}. Plots of intensities of the peak at $\delta = 163.1$ ppm versus contact time from the ^{13}C CP/MAS spectra for three neat block copolymers are given in Fig. 11. In this figure, comparisons are made between the experimental data (symbols) and the best fit curves (solid lines) obtained from an optimization with Eq. (2) having two adjustable parameters (M_0 and T_{CH}) for three neat S2VP diblock copolymers. In determining values of T_{CH} by curve fitting, we compared the differences between experimental data and curve-fit values and then minimized the root-mean-square of the sum of the differences between experimental data and curve-fit values. The values of T_{CH} thus determined are summarized in Table 5.

Peak intensities are normally measured from the peak height, based on the reasonable assumption that the peak widths are constant. Due to the weak peak intensities of the *ipso* carbon resonance of P2VP at $\delta = 163.1$ ppm for the S2VP-5 and S2VP-25 samples, we observed quite a bit of scatter in the data, especially for the former sample. Therefore, the NMR signal averaging time was 25 times longer for sample S2VP-5 than for S2VP-25 in order to detect the 163.1 ppm signal. For S2VP-5, (S2VP-5)/Cloisite 30B® and (S2VP-25)/Cloisite 30B® nanocomposite samples, to obtain a higher signal-to-noise ratio for the *ipso* carbon of the P2VP block we represented $M(t)$ by a plot of signal intensity obtained by integration of the region from $\delta = 156$ to 168 ppm versus contact time, instead of the simple peak intensity versus contact time used for the fits of the remainder of the peaks. Plots of $M(t)$ versus contact

Table 5
Values of T_{CH} determined from curve fitting the variable contact time.

Sample code	T_{CH} (μs)				
	Peak position δ (ppm)				
	163.1	145.8	133.9	125.0	40.6
S2VP-5	150	400		136	99
(S2VP-5)/Cloisite 30B®	108 ± 9	316		85.3	70
S2VP-25	520	510		80	57
(S2VP-25)/Cloisite 30B®	290 ± 20	350 ± 10		71 ± 0	59 ± 2
S2VP-56	500	140	53	66	60
(S2VP-56)/Cloisite 30B®	520	210	42	59	52

Data were processed using Excel spreadsheet with the two-parameter fit protocol, and reported errors are calculated standard deviations.

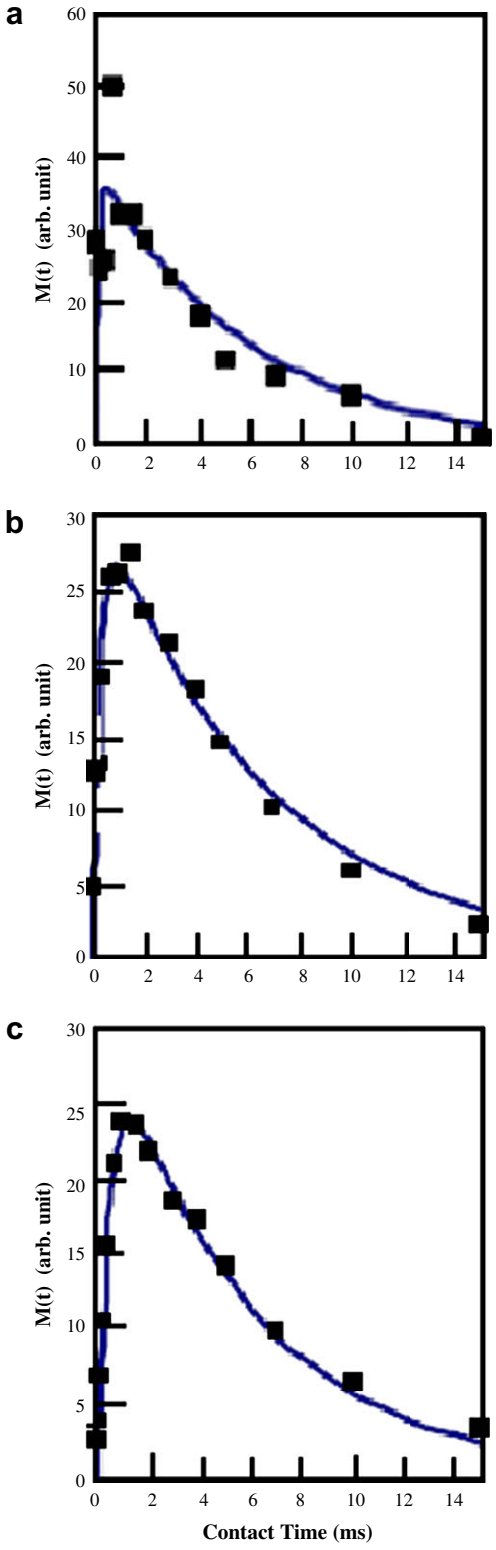

Fig. 12. Plots of $M(t)$ of ^{13}C CP/MAS spectra at $\delta = 163.1$ ppm versus contact time for (a) (S2VP-5)/Cloisite 30B® nanocomposite, (b) (S2VP-25)/Cloisite 30B® nanocomposite, and (c) (S2VP-56)/Cloisite 30B® nanocomposite, in which the symbols represent experiment data and the solid lines represent the best fit from Eq. (2) from the Excel fitting procedure described in the text.

time for three nanocomposites are given in Fig. 12, in which comparison is made between the experimental data (symbols) and the best fit curves (solid lines) obtained from an optimization with Eq. (2) having two adjustable parameters (M_0 and T_{CH}) using the same curve fitting procedure as described above. The values of T_{CH} thus determined are also summarized in Table 5.

At this juncture we wish to elaborate on the method of detecting *ipso* carbon signal intensities from S2VP-5 in Fig. 9a. The relaxation characteristics of the signal from the *ipso* carbon in all three block copolymers are critical to the NMR arguments for the existence of binding to the surface (and exfoliation of the clays). The signal-to-noise ratios (S:N) of these signals (163.1 ppm) in the spectra from S2VP-56 and S2VP-25 were 25 and 10; their height at the peak maximum yielded good plots and fits to biexponential relaxation curves (Fig. 12b and c). There is a hint of a signal from the *ipso*-2VP carbon in the spectrum of S2VP-5 shown Fig. 9a. Based on the spectra of the other polymers, we expect the S:N at the peak maximum to be ca. 2:1 if the same number of transients is accumulated. For this sample, the spectra were accumulated for ca. 25 times longer than the data accumulation times used for S2VP-25 and S2VP-56 samples, providing a 5-fold increase in S:N. Thus, the signal strength of the *ipso*-2VP from S2VP-5 was similar to the corresponding resonance in sample S2VP-25. We can achieve additional benefits of signal averaging by adding the intensities of all the points along the peak shape (this is the peak integral). Indeed, an excellent fit of integral value versus contact time to biexponential plots is achieved in Fig. 12a, confirming the validity of the methodology.

The following observations are worth noting in Table 5. While there is little or no change in the value of T_{CH} of the PS block (at $\delta = 145.8$ ppm) before and after mixing with an organoclay, the value of T_{CH} of the P2VP block (at $\delta = 163.1$ ppm) has decreased significantly from 150 to 108 ± 9 μs for the (S2VP-5)/Cloisite 30B® nanocomposite, indicating that the polar group in the P2VP segments of S2VP-5 in the nanocomposite must have interacted via ion–dipole interactions, with the positively charged N^+ ion in the surfactant MT2EtOH residing at the surface of Cloisite 30B®. This observation now explains why the (S2VP-5)/Cloisite 30B® nanocomposite has a very high degree of dispersion (near exfoliation) of the aggregates of Cloisite 30B® (see the TEM image given in Fig. 2b), confirming the hypothesis made above of the presence of ion–dipole interactions in the nanocomposite. Notice, however, in Table 5 that the value of T_{CH} for P2VP block in the (S2VP-25)/Cloisite 30B® nanocomposite has decreased moderately from 520 to 290 ± 20 μs. The degree of reduction for S2VP-25 is similar to that of S2VP-5, indicating somewhat significant interaction with the Cloisite 30B®. Nevertheless, we already observed that the (S2VP-25)/Cloisite 30B® nanocomposite has a lesser degree of dispersion of the aggregates of Cloisite 30B® (see the TEM image given in Fig. 2e). However, there is essentially no change in T_{CH} for S2VP-56 upon mixing with Cloisite 30B® indicating that for most of the 2VP moieties in this sample there is

Table 6
Values of T_{CH} determined from curve fitting the variable contact time in repeated NMR experiments for (S2VP-25)/Cloisite 30B®.

Sample code (S2VP-25)/Cloisite 30B®	T_{CH} (μs)				
	Peak position δ (ppm)				
	163.1	145.8	133.9	125.0	40.6
Run 1	270	360		71	57
Run 2	302	346		71	60
Mean value	286	353		71	58.5
Sample standard deviation	22.6	9.9		0	2.1
% Error	7.9	2.8			3.6

Data were processed using Excel spreadsheet with the two-parameter fit protocol.

Table 7
(S2VP-5)/Cloisite 30B relaxation measurement error analysis of NMR experiments.

Sample code	Integral region	T_{CH} (μs)
Region 1	177.0–162.5 ppm	114
Region 2	177.0–162.0 ppm	111
Region 3	177.0–161.5 ppm	108
Region 4	177.0–161.0 ppm	105
Region 5	177.0–161.0 ppm	102
Mean value		108
Sample standard deviation		8.5
% Error		7.9

Data were processed using Excel spreadsheet with the two-parameter fit protocol.

little or no surface interaction in the sample (see the TEM image given in Fig. 2h). This observation suggests that the majority, if not all, of the polar groups in the P2VP block of S2VP-56 must have self-associated.

In order to evaluate the errors of the relaxation time measurements, sample (S2VP-25)/Cloisite 30B® was measured twice on different dates. Relaxation T_{CH} data, the mean and the sample standard deviation values as well as the percent relative errors are listed in Table 6. The experimental results show that the T_{CH} values of this sample are 290 ± 20, 350 ± 10, 71 ± 0, and 59 ± 2 for the carbon atoms at $\delta = 163.1$, 145.8, 125.0, and 40.6 ppm, respectively. The relative experimental measurement errors are therefore 8%, 3%, 0%, and 4% for the carbon atoms at $\delta = 163.1$, 145.8, 125.0, and 40.6 ppm, respectively.

In order to evaluate the errors from data processing, 5 integration areas were chosen for the quaternary carbon signal of the 2VP segments from sample (S2VP-5)/Cloisite 30B®. Data were then processed in an Excel spreadsheet with the two-parameter fit protocol. Relaxation T_{CH} data, the mean and the sample standard deviation values as well as the percent relative errors are listed in Table 7. By choosing integral areas that progressively expanded toward the intense upfield aromatic signals, the impact of these signals on the relaxation characteristics of the *ipso* carbon of the 2VP segments in the copolymer was simultaneously evaluated. It was found that the intense upfield signal made contributions within the relative experimental error (8%) of the measurements. Based on rigorous statistical analysis, the values of T_{CH} for samples (S2VP-5)/Cloisite 30B® and (S2VP-25)/Cloisite 30B® are different at the 90–95% confidence level.

4. Concluding remarks

In this paper, we have shown that properly designed block copolymers without chemical modification can give rise to exfoliated organoclay nanocomposites. Specifically, we synthesized a series of S2VP diblock copolymers with various block compositions. We found that an S2VP diblock copolymer with 5 wt% P2VP block (S2VP-5) has exfoliated four different organoclays, regardless of the differences in chemical structures of the surfactant residing at the surface of the organoclays. We hypothesized that the experimentally observed dispersion characteristics of the nanocomposites are attributable to the presence of ion–dipole interactions between the positively charged N^+ ion in the surfactant residing at the surface of organoclay and the polar pyridine rings in the P2VP block of S2VP-5. However, we observed that the nanocomposite based on S2VP-5 with MMT showed a very poor dispersion of MMT aggregates. Interestingly, we have found that the degree of dispersion of organoclay aggregates became progressively poorer as the amount of P2VP block in S2VP diblock copolymer was increased from 5 to 25 and to 56 wt%.

Using solid-state NMR spectroscopy we have shown that indeed there were ion–dipole interactions between the positively charged N^+ ion in the surfactant residing at the surface of organoclay and the dipoles in the P2VP block of S2VP diblock copolymers. Not only we have shown the presence of ion–dipole interactions in the organoclay nanocomposites based on P2VP-containing block copolymers, but we have also been able to explain the reasons why the block length ratio of S2VP diblock copolymer in the organoclay nanocomposites played a significant role in determining the extent of dispersion of organoclay aggregates in the nanocomposites. The results of our solid-state NMR spectroscopy have indicated that there exists an optimum range of the amount of functional P2VP block in an S2VP diblock copolymer that can give rise to exfoliation of organoclay aggregates. That is, an excessive amount of a functional block in a block copolymer will preferentially induce intramolecular interactions (self-association), hindering intermolecular interactions with a surfactant residing at the surface of an organoclay, giving rise to poorly dispersed organoclay aggregates. To our knowledge, no such investigation, experimental or theoretical, on ion–dipole interactions in organoclay nanocomposites has ever been reported in the literature.

Acknowledgment

C.D. Han acknowledges with gratitude that this study was supported in part by the National Science Foundation under Grant CST-0406752. J.K. Kim acknowledges the support of the National Creative Research Initiative Program by the Korea Science and Engineering Foundation (KOSEF). Synchrotron small-angle X-ray scattering and XRD experiments were performed at PLS beamlines 4C1 and 10C1, respectively, supported by POSCO and KOSEF. P.L. Rinaldi wishes to thank the Kresge Foundation and donors to the Kresge Challenge Program at the University of Akron for funds used to purchase the NMR instrumentation used in this work. We wish to thank the staff of the University of Akron Magnetic Resonance Center for providing access to NMR related capabilities used in this work.

References

[1] Ray SS, Okamoto M. Prog Polym Sci 2003;28:1539.
[2] Lee KM, Han CD. Macromolecules 2003;36:804.
[3] Choi S, Lee KM, Han CD. Macromolecules 2004;37:7649.
[4] Zha W, Choi S, Lee KM, Han CD. Macromolecules 2005;38:8418.
[5] Ha YH, Kwon Y, Breiner T, Chan EP, Tzianetopoulou T, Cohen RE, et al. Macromolecules 2005;38:5170.
[6] Di J, Sogah DT. Macromolecules 2006;39:5052.
[7] Mitchell CA, Krishnamoorti R. J Polym Sci Polym Phys Ed 2002;40:1434.
[8] Chen H, Schmidt DF, Pitsikalis M, Hadjichristidis N, Zhang Y, Wiesner U, et al. J Polym Sci Polym Phys Ed 2003;41:3264.
[9] Silva AS, Mitchell CA, Tse MF, Wang HC, Krishnamoorti R. J Chem Phys 2001;115:7166.
[10] Krishnamoorti R, Silva AS, Mitchell CA. J Chem Phys 2001;115:7175.
[11] Ha YH, Thomas EL. Macromolecules 2002;35:4419.
[12] Liao M, Zhu J, Xu H, Li Y, Shan W. J Appl Polym Sci 2004;92:3430.
[13] Hasagawa N, Usuki A. Polym Bull (Berlin) 2003;51:77.
[14] Bockstaller MR, Mickiewicz RA, Thomas EL. Adv Mater 2005;17:1333.
[15] Physical properties bulletin from southern clay products.
[16] Lee KM, Han CD. Macromolecules 2003;36:7165.
[17] Stejskal EO, Memory JD. High resolution NMR in the solid state, fundamentals of CP/MAS. New York: Oxford University Press; 1994.
[18] Chu CW, Dickinson LC, Chien JCW. J Appl Polym Sci 1990;41:2311.
[19] Schmidt-Rohr K, Clauss J, Spiess HW. Macromolecules 1992;25:3273.
[20] Jack KS, Whittaker AK. Macromolecules 1997;30:3560.
[21] Takegoshi K, Hikichi K. J Chem Phys 1991;94:3200.
[22] Fyfe CA. Solid state NMR for chemists. Guelph, Ontario, Canada: C.F.C Press; 1983.
[23] Yoon PJ, Hunter DL, Paul DR. Polymer 2003;44:5323.
[24] Chavarria F, Paul DR. Polymer 2006;47:7760.
[25] Leibler L. Macromolecules 1980;13:1602.
[26] Hara M, Eisenberg A. Macromolecules 1984;17:1335.
[27] Hara M, Eisenberg A. Macromolecules 1987;20:2160.
[28] Parker G, Hara M. Polymer 1997;38:2701.
[29] Lim JC, Park JK, Song HY. J Polym Sci Polym Phys Ed 1994;32:29.
[30] Mehring M. NMR basic principles and progress, vol. 11. Berlin: Springer; 1976.